Edinburgh, Scotland
EURONOISE 2009
October 26-28

Effective acoustical properties of random microfibrous materials

Rodolfo Venegas[a]
Olga Umnova[b]
Acoustics Research Centre, University of Salford, UK.

ABSTRACT

Fibrous materials have been traditionally modelled as arrays of regularly-placed circular cylinders in which rarefaction effects are not considered. These effects should be taken into account when a characteristic pore/inclusion size of the material becomes comparable to the mean molecular free path. Therefore, the oscillatory Stokes forced and heat transfer problems have to be solved considering slip and temperature-jump boundary conditions on the solid boundaries to estimate viscous and thermal losses. In this paper effective acoustical quantities, such as speed of sound and attenuation coefficient, of random microfibrous materials are studied numerically. The material geometry is constructed by using the Metropolis method for canonical equilibrium ensembles with periodic boundary conditions. Different array porosities and Knudsen number values are considered. Finally, classical semi-phenomenological models are discussed and modified to describe viscous and thermal losses in the abovementioned materials.

1. INTRODUCTION

Plane wave propagation in a homogenous medium can be fully described through two quantities: the wave number k_c and the characteristic impedance Z_c. A porous medium can be modeled as an equivalent fluid when the wavelength largely exceeds the characteristic pore/inclusion size. The viscous and thermal losses are accounted for by means of the dynamic density $\rho(\omega)$ and the dynamic bulk modulus $K(\omega)$, both being complex and frequency dependent functions[1]. These intrinsic properties are related to dynamic viscous $k(\omega)$ and thermal $k'(\omega)$ permeabilities. They can be calculated from the solution of the oscillatory fluid flow and thermal problems through the dynamic extension of the Darcy's law[2] and an analogous Darcy's thermal law[3] respectively. Different approaches to characterizing porous materials have been proposed. One of them consists in calculating dynamic permeabilities from their definition (microstructural or direct calculation henceforth). A second approach relies on using semi-phenomenological models. These models are based on scaling functions which depend on macroscopic independently measurable parameters to describe dynamic viscous and thermal permeabilities[3,4,5,6,7]. Despite their wide use, semi-phenomenological models cannot be directly applied to sound propagation in a confined space. Therefore, they should be modified when applied to describe acoustical properties of microporous materials. To properly describe frequency-dependent viscous and thermal losses in these materials, the oscillatory Stokes

[a] Email address. r.g.venegascastillo@pgr.salford.ac.uk
[b] Email address. o.umnova@salford.ac.uk

forced and heat transfer problems have to be solved considering Knudsen and temperature-jump boundary conditions on the solid boundaries. These two problems have been analytically solved by Kozlov et al.[8] for straight pores of different shape. Although the significance of their work is undoubtedly a cylindrical-pore approximation seems to be too basic for fibrous materials. Historically, they have been modeled as arrays of circular cylinders. Numerous analytical solutions for acoustical properties of regular arrays of cylinders, namely square and hexagonal lattices, have been proposed by different authors[9,10,11,12,13]. They have proven to give reasonable agreement with experimental data. However, spatial regularity is rarely found in real materials. In this work, a modified semi-phenomenological model is proposed to investigate the slip/temperature-jump influence on sound speed $c(\omega)$ and attenuation coefficient $a_t(\omega)$ of random mono-disperse arrays of circular cylinders. Different array porosities ϕ and Knudsen number, $K_n = l_{mean}/r$, values are considered. The proposed modified model reduces to the classical one when the characteristic pore/inclusion size is much larger than the mean free molecular path l_{mean} of the saturating fluid. The arrays are generated using the Metropolis method for canonical equilibrium ensembles with periodic boundary conditions[14]. A representative number of these arrays are used to calculate mean effective acoustical quantities and all the macroscopic parameters involved in the modified model. These parameters are compared to the analytical solution and numerical results for a regular array of cylinders arranged in square lattice[15]. The presence of some effects previously observed in random arrays of cylinders under negligible confined effects[16] is also investigated in microfibrous materials. The paper is organized as follows. In section II, the theory and methods are described. Section III presents results and discussion. Concluding remarks are presented in section IV.

2. THEORY AND METHODS

A. Oscillatory Stokes forced problem with slip boundary condition

Consider a homogenous rigid porous medium saturated by a Newtonian fluid of viscosity η, density ρ_0 and porosity ϕ. Its characteristic pore/inclusion size is comparable to the mean molecular free path, i.e. $r = O(l_{mean})$. The long-wavelength linear response to a macroscopic harmonic small-amplitude pressure gradient $\nabla p e^{j\omega t}$ with angular frequency ω can be obtained from the solution of the oscillatory Stokes forced problem [equations (1) and (2)]. This problem has been derived using homogenization theory accounting for the slip phenomenon in reference[17]. Assuming separation of scales between the macroscopic characteristic length L and either a physical quantity involved in the problem or a characteristic size l of the porous medium, an expansion parameter $\varepsilon = l/L$ can be defined. Thus, the existence of a representative elementary volume (REV Ω) in which the problem is solved can also be ensured. The dimensionless equations at the microscopic level (order ε^1) derived in reference[17] are recalled

$$\eta \nabla_y^2 \mathbf{u}^{(0)} - \nabla_x p^{(0)} - \nabla_y p^{(1)} = j\omega\rho \mathbf{u}^{(0)} \qquad \text{and} \qquad \nabla_y \cdot \mathbf{u}^{(0)} = 0 \qquad \text{in } \Omega_f \tag{1}$$

$$\mathbf{u}^{(0)} = -K_n \left(\mathbf{t}_1^{(0)} \cdot \nabla_y \mathbf{u}^{(0)} \cdot \mathbf{n} \right) \mathbf{t}_1^{(0)} \qquad \text{on } \Gamma' \tag{2}$$

where $\mathbf{t}_1^{(0)}$ and $\mathbf{n}$ are the unitary vectors tangential and normal to Γ'. Subscripts y and x denote microscopic and macroscopic dimensionless space variable respectively (see Chastanet et al.[17] for more detail). Periodic boundary conditions for velocity and pressure on the REV's boundaries are also applied. The dynamic extension of the Darcy's law [equation (3)] provides a way of calculating the dynamic permeability tensor including slip effects $\mathbf{k}(\omega, K_n) = \langle \mathbf{k}(y, \omega, K_n) \rangle$.

$$\langle \mathbf{u}^{(0)} \rangle = -\frac{\langle \mathbf{k}(y, \omega, K_n) \rangle}{\eta} \nabla_x p^{(0)} \tag{3}$$

where the average is taken over the fluid phase $\langle\cdot\rangle = \int_{\Omega_f} \cdot d\Omega / |\Omega|$ and $|\Omega|$ is a spatial measure, e.g. area or volume, of the REV[17]. For isotropic materials or if one considers a preferential flow direction the dynamic viscous permeability tensor becomes a scalar quantity $k(\omega, K_n)$. The complex frequency-dependent dynamic density function $\rho(\omega, K_n)$ is related to dynamic viscous permeability and dynamic tortuosity $\alpha(\omega, K_n)$ as follows:

$$\rho(\omega, K_n) = \alpha(\omega, K_n)\rho_0 = \eta\phi / j\omega k(\omega, K_n) \tag{4}$$

B. Oscillatory heat transfer problem with temperature-jump boundary condition

Consider an isothermal solid frame saturated by a fluid with thermal conductivity κ, specific heat at constant pressure C_p and specific heat ratio γ. The temperature distribution can be calculated from the solution of an oscillatory heat transfer problem given by equation (5). Under confinement, the temperature on the solid boundaries can no be longer considered zero. Instead the temperature-jump boundary condition should be used, i.e. temperature on the solid boundaries is proportional to the temperature flux (equation (6)).

$$j\omega\rho C_p \tau^{(0)} = \kappa \nabla_y^2 \tau^{(0)} + j\omega p^{(0)} \qquad \text{in } \Omega_f \tag{5}$$

$$\tau^{(0)} = \frac{2\gamma}{(\gamma+1)} \frac{K_n}{N_{pr}} \nabla_y \tau^{(0)} \cdot \mathbf{n} \qquad \text{on } \Gamma' \tag{6}$$

where $N_{pr} = C_p \eta / \kappa$ is the Prandtl number.

Lafarge et al[3]. have derived an analogous dynamic thermal Darcy's law using homogenization theory. However, the thermal slip influence has not been taken into account in their work. Based on findings of references[8,15], this law may be extended to account for slip influence as is shown in equation (7)

$$\left\langle \tau^{(0)} \right\rangle = \frac{j\omega \left\langle k'(y, \omega, K_n) \right\rangle}{\kappa} p^{(0)} \tag{7}$$

The dynamic bulk modulus $K_a(\omega, K_n)$ is related to dynamic thermal permeability $k'(\omega, K_n)$ and compressibility $C(\omega, K_n)$ as follows:

$$K_a(\omega, K_n) = \frac{\gamma P_0}{C(\omega, K_n)} = \gamma P_0 \left(\gamma - j\omega\rho_0(\gamma - 1) \frac{C_p k'(\omega, K_n)}{\kappa\phi} \right)^{-1} \tag{8}$$

where P_0 the is atmospheric pressure. Periodic boundary conditions for temperature on the REV's boundary are also applied.

C. Scaling function for dynamic viscous permeability

Johnson et al[5]. proposed a scaling function to calculate dynamic viscous permeability. This function matches two leading terms at high frequencies but only the first term at low frequencies. Pride et al.[6] noted that Johnson et al.[5] model is not sufficiently accurate in the frequency range where both viscous and inertial interactions are of the same order. They proposed a more accurate scaling function which preserves the two leading terms at both low and high frequency limits. The expression for the dynamic viscous permeability proposed by Pride et al.[6] depends on porosity ϕ, viscous permeability k_0, static tortuosity α_0', viscous characteristic length Λ and tortuosity α_∞. It is given by equation (9).

$$k(\omega) = k_0 \left(j\frac{\omega}{\omega_v} + \left(1 - P_v + P_v \sqrt{1 + j\frac{\omega}{\omega_v}\left(\frac{M_v}{2P_v^2} \right)} \right) \right)^{-1} \tag{9}$$

where $P_v = M_v / 4(\alpha_0 / \alpha_\infty - 1)$; $M_v = 8k_0\alpha_\infty / \phi\Lambda^2$ is the viscous shape factor and $\omega_v = \eta\phi / \alpha_\infty k_0 \rho_0$ is the viscous characteristic frequency.

The Knudsen number-dependent viscous permeability, $k_0(K_n)$, is calculated from the solution of equations (1), setting frequency equal to zero, and (2) by means of equation (3). Static viscous tortuosity is given by $\alpha_0(K_n) = \mathrm{Re}\{\alpha(K_n, \omega \to 0)\}$. At high frequencies, viscosity effect can be neglected and the fluid flow satisfies the Laplace equation (potential flow)[5]. Brown[18] has noted that the same type of equation also describes the electrical conduction problem for a porous medium in which the solid phase is insulating and the saturating fluid is conducting. Therefore, the limiting fluid flow problem can be posed as an electrical one in which the scaled electric field gives the solution for the fluid high-frequency flow problem. This is given by:

$$\nabla^2 \vartheta = 0 \quad \text{in } \Omega_f \qquad \mathbf{n} \cdot \nabla \vartheta = \mathbf{n} \cdot \mathbf{e} \quad \text{on } \Gamma \tag{10}$$

where $\mathbf{n}$ is the unit normal pointing outward from the pore region and ϑ is the deviatoric part of an electric potential. The latter is related to the scaled electric field (local electrical field divided by the applied macroscopic potential gradient) as $\mathbf{E} = \mathbf{e} - \nabla \vartheta$ (Hodge decomposition); $\mathbf{e}$ being the unit electric field. Periodic boundary conditions on the REV's boundaries are also applied. If one considers an isotropic material or a preferential flow direction, tortuosity α_∞ and viscous characteristic length Λ can be calculated as follows:

$$\alpha_\infty = \left|\Omega_f\right| \left(\int_{\Omega_f} (\mathbf{e} - \nabla \vartheta) \cdot \mathbf{e} \, d\Omega \right)^{-1} \qquad \Lambda = 2 \int_{\Omega_f} \left|\mathbf{e} - \nabla \vartheta\right|^2 d\Omega \left(\int_{\Gamma} \left|\mathbf{e} - \nabla \vartheta\right|^2 d\Gamma \right)^{-1} \tag{11}$$

It has been found[8,15] that high-frequency macroscopic parameters do not depend on Knudsen number.

D. Scaling function for dynamic thermal permeability

Lafarge et al.[3,4] have introduced the following scaling function to calculate dynamic thermal permeability.

$$k'(\omega) = k_0' \left(j \frac{\omega}{\omega_t} + \left(1 - P_t + P_t \sqrt{1 + j \frac{\omega}{\omega_t} \left(\frac{M_t}{2 P_t^2} \right)} \right) \right)^{-1} \tag{12}$$

where $P_t = M_t / 4(\alpha_0' - 1)$. $M_t = 8 k_0' / \phi \Lambda'^2$ is the thermal shape factor and $\omega_t = \kappa \phi / C_p \rho_0 k_0'$ is the thermal characteristic frequency.

The static temperature distribution $\tau_{0,K_n}^{(0)}$ is calculated from the solution of a modified equation (5) and (6). The modification consists in setting the left-hand side to zero and the term $j\omega p^{(0)}$ is replaced by $p^{(0)}$. The Knudsen number-dependent thermal permeability is related to the static temperature distribution through $k_0'(K_n) = \kappa \left\langle \tau_{0,K_n}^{(0)} \right\rangle / p^{(0)}$. Static thermal tortuosity is given by $\alpha_0'(K_n) = \left\langle (\tau_{0,K_n}^{(0)})^2 \right\rangle \left\langle \tau_{0,K_n}^{(0)} \right\rangle^{-2}$. Finally, the thermal characteristic length[7] Λ' is a geometrical parameter equal to twice the volume-to-pore-surface ratio, i.e. $\Lambda' = 2 \int d\Omega \cdot \left(\int d\Gamma \right)^{-1}$.

E. Acoustical properties

The acoustic behaviour of a porous material is completely determined by the wave number $k_c(\omega, K_n)$ and the characteristic impedance $Z_c(\omega, K_n)$[1]. They both are functions of frequency and Knudsen number and are related to dynamic density and dynamic bulk modulus as follows:

$$k_c(\omega, K_n) = \omega \sqrt{\rho(\omega, K_n) K_a^{-1}(\omega, K_n)} \qquad Z_c(\omega, K_n) = (1/\phi) \sqrt{\rho(\omega, K_n) K_a(\omega, K_n)} \tag{13}$$

Speed of sound, $c(\omega, K_n)$, in the porous material and attenuation coefficient, $a_t(\omega, K_n)$ are given by:

$$c(\omega, K_n) = \omega / \mathrm{Re}\{k_c(\omega, K_n)\} \qquad a_t(\omega, K_n) = -\mathrm{Im}\{k_c(\omega, K_n)\} \tag{14}$$

F. Generation of the microfibrous material geometries (REV)

The random arrays, which correspond to the representative elementary volume REV, are constructed by using the Metropolis method for Gibbs ensembles (equilibrium ensembles). A detailed explanation of this method can be found in reference[14]. Only the key steps of the algorithm are delineated here. The method requires an initial configuration of N cylinders characterized by their centre coordinates and arranged in a given lattice. Then, one perturbs every cylinder centre with two random uniformly-distributed variables within the range $[-b,b]$, i.e. the cylinders can freely move throughout the REV of side length $2b$. The next step consists of checking the distances between the cylinders in order to avoid overlap. This is done considering a certain tolerance. If there is no overlap, the movement is accepted otherwise the cylinder returns to its previous position. Finally, periodic boundary conditions are implemented to reduce finite-size effects.

G. Numerical method (FEM)

The finite element method (FEM) has been employed for solving all the equations in this work. The FEM software Comsol Multiphysics[19] has been used. Second-order Lagrangian elements have been used to model the velocity components and temperature distribution, whereas linear elements approximated the pressure field. The elements were chosen so that a good enough resolution of the geometry is always achieved. A mesh refining analysis has been performed to ensure the convergence of the solutions. The slip boundary conditions have been implemented in the aforementioned software. More details can be found in reference[15].

3. RESULTS AND DISCUSION

A square regular lattice composed by 361 cylinders of radius r has been selected as the starting lattice to generate 30 random configurations for a Knudsen number $K_n = 0.05$ ($r = 1.2$ μm considering a $l_{mean} = 60$ nm). This has been done for porosity values ranging from 0.65 to 0.95 in steps of 0.1. The random geometries have been spatially scaled to generate the configurations for $K_n = 0.1$ and $K_n = 0.3$ (radii equal to 0.6 and 0.2 μm respectively). Figure 1 shows the static y-component fluid velocity (top) and static temperature distribution (bottom) of four arbitrary selected random configurations for porosities 0.65 to 0.95 (left to right) and $K_n = 0.05$. The gradient of pressure for the fluid flow problem has been applied in the negative y-axes direction. This exemplifies the type of geometries generated with the Metropolis method.

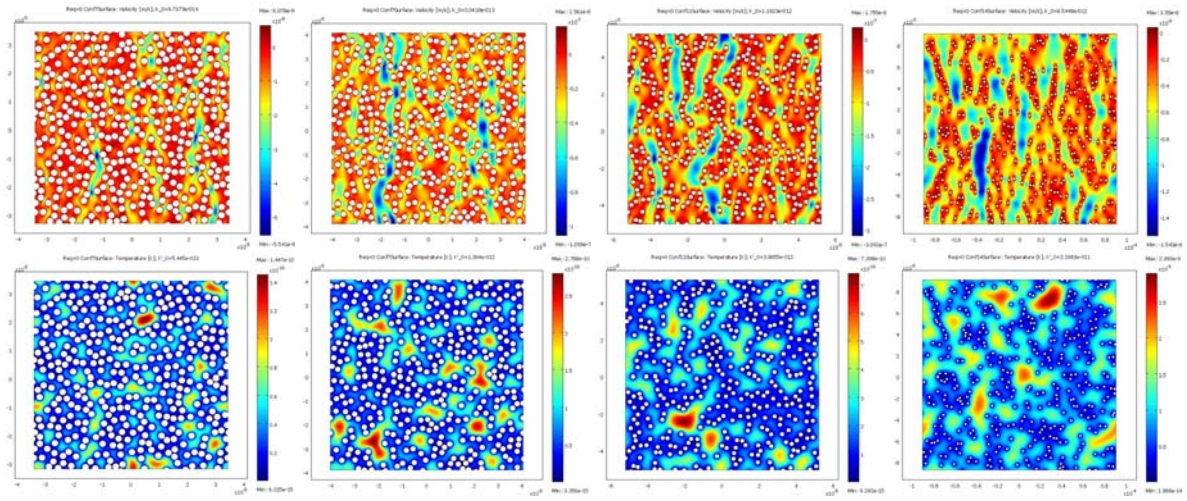

Figure 1: Static y-component of the fluid velocity (top) and static temperature distribution (bottom) for porosities from 0.65 to 0.95 (left to right) for $K_n = 0.05$.

Figure 2 shows dimensionless viscous (top) and thermal (bottom) permeabilities as function of porosity for three Knudsen number values 0.05, 0.1 and 0.3 (left to right). The red line represents the average value taken over 30 random configurations. The black line corresponds to the numerical solution for an array of micro cylinders arranged in a square lattice. This is referred to regular configuration from now on. Blue dots correspond to the analytical solution for the regular configuration[15].

It can be seen that for high porosity arrays the numerical and the analytical solutions for regular configurations are close each other. However, the analytical solution has a slightly different value compared to the numerical result at porosity 0.65. The numerical result is more accurate in this case. This disagreement for denser arrays has been explained in detail in reference[15].

In random arrays the mean value of viscous permeability is greater than that of regular arrays, $\overline{k_0^{ran}(K_n)} > k_0^{reg}(K_n)$ for $\phi > \phi_c$, where the critical porosity value is $\phi_c \approx 0.74$. For denser arrays, $\phi < \phi_c$, the opposite trend has been found $\overline{k_0^{ran}(K_n)} < k_0^{reg}(K_n)$. The same tendency and critical porosity value has been observed in random materials under negligible confinement[16]. This suggests that the critical porosity is related to the spatial distribution of the fibers and not to the scale.

Thermal permeability of random materials presents higher values than that of the ordered ones over the whole range of porosity studied in this paper i.e. $k_0'^{ran}(K_n) > k_0'^{reg}(K_n)$. This has also been observed in reference[16]. Static viscous tortuosity for random materials is larger than for regular materials $\alpha_0^{ran}(K_n) > \alpha_0^{reg}(K_n)$. This means that random materials exhibit larger effective fluid-inertia enhancement at low frequencies. Similar behaviour is identified in the case of static thermal tortuosity $\alpha_0'^{ran}(K_n) > \alpha_0'^{reg}(K_n)$. It is worth noting that all these parameters are affected by the slip condition.

High-frequency parameters, i.e. tortuosity and characteristic lengths, are not influenced by the slip condition[8,15]. This is expected since tortuosity is a geometrical parameter which does not depend on scale. In addition, it is a deterministic function of porosity and pore/inclusion shape for regular configurations. In random materials, tortuosity depends on porosity, the spatial distribution and the pore/inclusion shape. It has been found that tortuosity for random materials is always greater than that of regular ones with the same porosity $\alpha_\infty^{ran} > \alpha_\infty^{reg}$. Viscous characteristic length for random configurations attains a slightly lower value than regular configurations. Thermal characteristic length does not depend on spatial distribution when dealing with non-overlapping configurations. Therefore, its value is the same for random and regular configurations which have the same porosity.

Figure 3 shows dynamic viscous (left) and thermal (right) permeabilities calculated directly along with their calculation obtained by using the modified semi-phenomenological model. The direct calculation has been obtained by solving equations (1) to (3) for the viscous case and equations (5) to (7) for the thermal one. This has been performed for a discrete set of frequencies. Their values have been carefully selected to appropriately cover the viscous and inertial regime for each configuration. Two configurations per porosity per Knudsen number have been considered, i.e. 24 randomly selected disordered configurations are studied. The modified model given by equations (9) and (12) has been used to calculate dynamic viscous and thermal permeabilities.

Despite the effect of boundary slip on dynamic viscous and thermal permeabilities, their universal scaling nature remains intact. This means that the expressions proposed by Pride et al.[6] and Lafarge et al.[3,4] can still be used, provided that low frequency macroscopic parameters are calculated considering slip and temperature-jump boundary conditions. This provides a faster way of characterizing the acoustic behaviour comparing to the direct calculation.

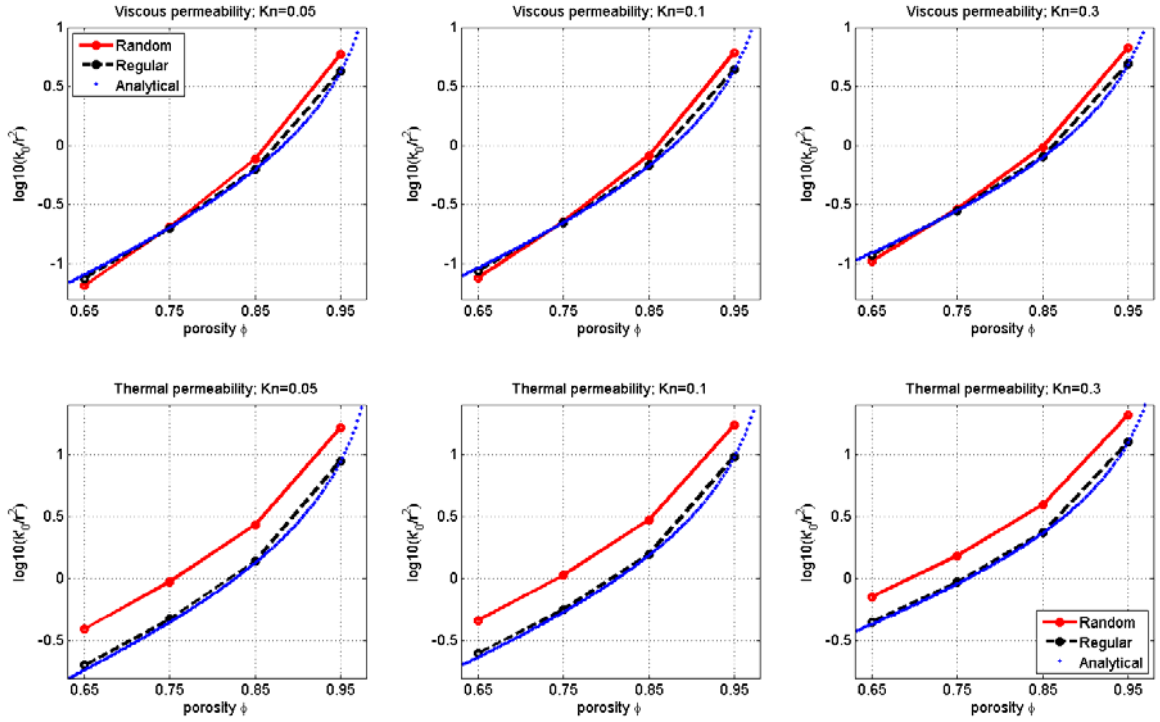

Figure 2: Dimensionless static viscous permeability (top) and thermal permeability (bottom) as function of porosity for Knudsen number values 0.05, 0.1 and 0.3 (left to right).

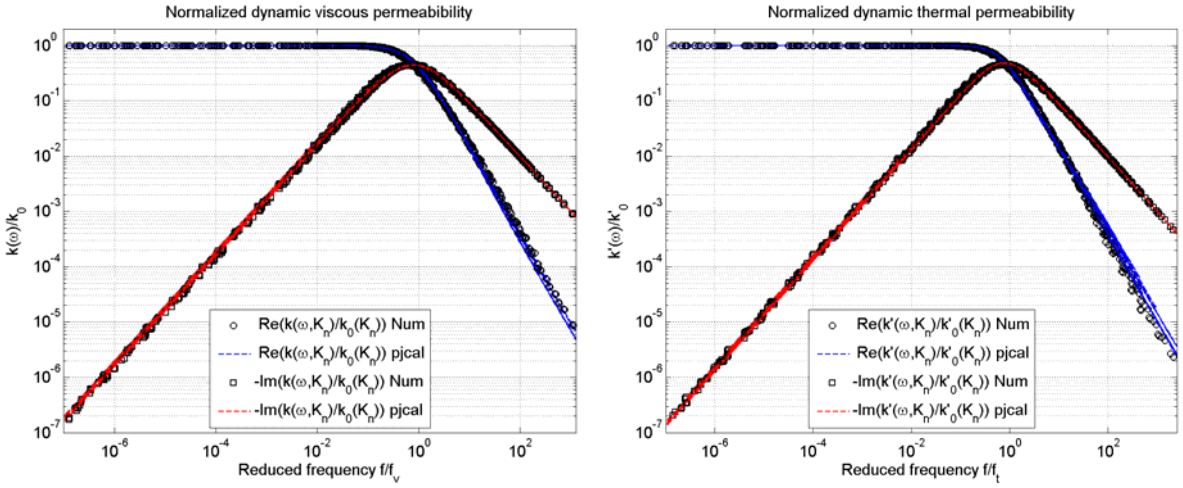

Figure 3: Normalized dynamic viscous (left) and thermal (right) permeabilities. Direct calculation (real part in black circles and imaginary part in black squares) and modified (pjcal) semi-phenomenological model (real part in blue lines, imaginary part in red lines).

Figure 4 shows mean value of attenuation coefficient (left) and normalized sound speed $c(\omega, K_n)/c_0$ (right) as function of the ratio between the cylinders radius and the boundary layer thickness $\Psi = r/\delta_v = r\sqrt{\rho_0 \omega / 2\eta}$ for different porosities and Knudsen numbers. The mean value has been taken over 30 random configurations per porosity (4 values) per Knudsen number (3 values).

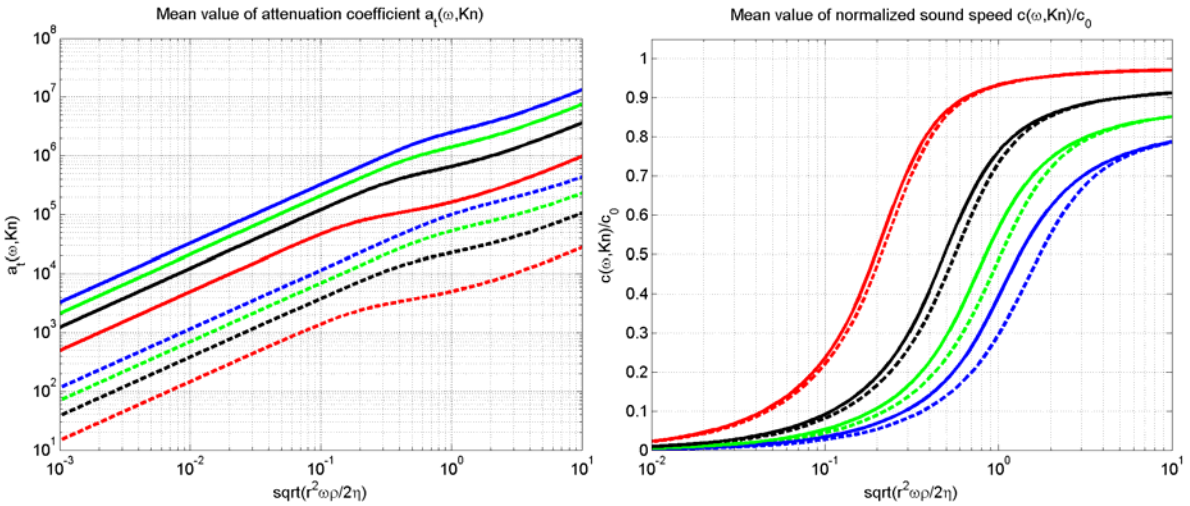

Figure 4: Mean value of attenuation coefficient (left) and sound speed (right) for porosities 0.65 (blue), 0.75 (green), 0.85 (black) and 0.95 (red). Knudsen numbers $K_n = 0.05$ (dashed line) and $K_n = 0.3$ (continuous line).

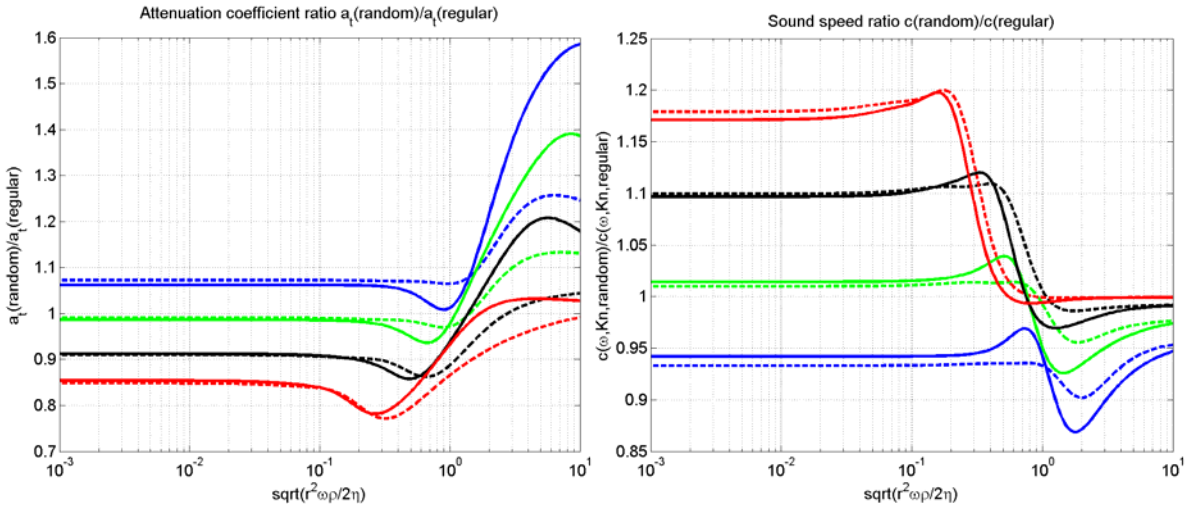

Figure 5: Attenuation coefficient (left) and sound speed (right) ratios for porosities 0.65 to 0.95 (blue, green, black and red). Knudsen numbers $K_n = 0.05$ (dashed line) and $K_n = 0.3$ (continuous line).

Attenuation coefficient is a monotonic increasing function of frequency. It has greater values for larger Knudsen numbers. In addition, it is larger for denser materials. Mean value of sound speed for $K_n = 0.05$ is smaller than that for $K_n = 0.3$ when $\Psi << 1$. This trend is more pronounced in the transition region, i.e. where viscous and inertial interactions are of the same order of magnitude. At high frequencies, sound speed tends to be the same asymptotic value, i.e. $c_0\left(\overline{\alpha_\infty^{ran}}\right)^{-1/2}$. This is due to the fact that the generated configurations possess the same spatial distribution and porosity, and also the inexistent slip influence at high frequencies. Regular configurations show the same trend for both attenuation coefficient and speed of sound. However, this is not shown here for the sake of brevity. See for example reference[15].

Figure 5 shows the ratio between the mean value of attenuation coefficient of random configurations and the attenuation coefficient of regular configuration (left). The ratio for sound speed is shown on the right side of this figure. The influence of the critical porosity is clearly identified in the region where $\Psi << 1$. Attenuation coefficient for random configurations is larger

than that of regular ones when $\phi < \phi_c$ for all Knudsen number values. The opposite trend is found when $\phi > \phi_c$.

The attenuation coefficient ratio becomes larger when Knudsen number diminishes for porosities $\phi < 0.85$ and $\Psi << 1$. For higher porosity configurations ($\phi > 0.85$), the opposite behaviour is observed at low frequencies, i.e. the deviation of the mean value of attenuation coefficient from that of the regular configurations is greater when Knudsen number increases. When $r \approx O(\delta_v)$ and Ψ is slightly greater than one, the attenuation coefficient ratio increases when the Knudsen number rises. Therefore, the spatial distribution of the fibres plays an important role when the fibre radius is of the order of the viscous boundary layer thickness for confined materials. Speed of sound ratio exceeds the unit when $\phi > \phi_c$ and $\Psi << 1$ for all Knudsen number values. The sound speed ratio is smaller when the Knudsen number diminishes for porosities $\phi < 0.85$ and $\Psi << 1$. When $r \approx O(\delta_v)$ and Ψ is slightly larger than one, the sound speed ratio shows a pronounced peak for larger Knudsen numbers and dense configurations. After this peak, the ratio starts decreasing for all Knudsen numbers and shows smaller values for more confined configurations. At the high-frequency limit, the configurations converge to the same value $\sqrt{\alpha_\infty^{reg} / \alpha_\infty^{ran}}$. This is independent of the scale.

4. CONCLUSIONS

A modified semi-phenomenological model has been proposed to investigate the slip/temperature-jump influence on acoustical properties of random microfibrous materials. The model has the same functional form as the original formulation[3-7]. However, the low frequency macroscopic parameters should be calculated considering slip and temperature-jump boundary conditions. This provides a faster way of characterizing the acoustic behaviour in comparison to the direct calculation. This is the central finding of this paper.

A critical porosity has been identified. In a random array the mean value of viscous permeability is greater than that for a regular array for porosities larger than the critical one, $\phi > \phi_c$. For denser arrays, $\phi < \phi_c$, the opposite trend has been found. The same tendency and critical porosity value has been observed in non-confined random materials[16]. This suggests that the critical porosity is related to the spatial distribution and not to the scale. This critical porosity clearly determines the acoustic behaviour of random microfibrous materials at low frequencies (viscous regime), i.e. the attenuation coefficient for random configurations is larger than that of regular ones when $\phi < \phi_c$ for all Knudsen number values. The opposite trend is found when $\phi > \phi_c$. In a similar way, speed of sound in random materials is greater than that in regular configurations for porosities larger than ϕ_c.The opposite behaviour is observed when $\phi < \phi_c$. In general, the spatial distribution of the fibres plays an important role when the fibre radius is of the order of the viscous boundary layer thickness for sound propagation in confined space.

ACKNOWLEDGMENTS

The author gratefully acknowledges ORSAS award and University of Salford research studentship.

REFERENCES

1. J. F. Allard. Propagation of Sound in Porous Media: Modeling Sound Absorbing Materials. Chapman & Hall, London, 1993.
2. J. Auriault, L. Borne and R. Chambon, Dynamics of porous saturated media, checking of the generalized law of Darcy, *J. Acoust. Soc. Am.* Vol. **77** (5). pp. 1641-1650, (1985).
3. D. Lafarge, P. Lemarinier, J.F. Allard and V. Tarnow, Dynamic compressibility of air in porous structures at audible frequencies, *J. Acoust. Soc. Am* **102** (4), pp. 1995-2006, (1997).

4. D. Lafarge, Propagation du son dans les matériaux poreux à structure rigide saturés par un fluide viscothermique, Ph. D. Thesis, Université du Maine, 1993 (Sound propagation in rigid porous media saturated by a viscothermal fluid)
5. D. L. Johnson, J. Koplik and R. Dashen, Theory of dynamic permeability and tortuosity in fluid-saturated porous media, *J. Fluid Mech.* **176**, pp. 379-402, (1987).
6. S. R Pride, F. D. Morgan and A.F. Gangi, Drag forces of porous-medium acoustics, *Phys. Rev. B* **47**, pp. 4964-4975, (1993).
7. Y. Champoux and J.F. Allard, Dynamic tortuosity and bulk modulus in air-saturated porous media, *J. Appl. Phys.* **70** (4), pp. 1975-1979, (1991).
8. V.F. Kozlov, A.V. Fedorov and N.D. Malmuth, Acoustical properties of rarefied gases inside pores of simple geometries, *J. Acoust. Soc. Am.* **117**, pp. 3402-3411, (2005).
9. J. F. Allard and Y. Champoux, New empirical equations for sound propagation in rigid frame fibrous materials. *J. Acoust. Soc. Am*., **91**, pp. 3346-3353, (1992).
10. K. Attenborough, Acoustic characteristics of rigid fibrous absorbents and granular materials, *J. Acoust. Soc. Am.* **73**, pp. 785–799, (1983).
11. V. Tarnow, Compressibility of air in fibrous materials, *J. Acoust. Soc. Am.* **99** (5), pp. 3010-3017, (1996).
12. V. Tarnow, Calculation of the dynamic air flow resistivity of fibre materials, *J. Acoust. Soc. Am.* **102** (3), pp. 1680-1688, (1997).
13. O. Umnova, K. Attenborough, K. M. Li, A Cell model for the acoustical properties of fibrous absorbents, in Proceedings of Inter-Noise 2000, Nice, 27-30 August 2000.
14. S. Torquato, Random Heterogeneous materials, Microstructure and Macroscopic properties, Interdisciplinary Applied Mathematics, Vol. 16 Springer Verlag, 2001.
15. O. Umnova, D. Tsiklauri and R. Venegas, Effect of boundary slip on the acoustical properties of microfibrous materials, accepted for publication in *J. Acoust. Soc. Am.* (2009)
16. R. Venegas and O. Umnova, Acoustical properties of disordered arrays of circular cylinders, in Proceedings of SAPEM 2008. Bradford, UK, December 17-18-19, 2008.
17. J.Chastanet, P.Royer and J.-L.Auriault, Acoustics with wall-slip flow of gas saturated porous media. *Mechanics Research Communications* **31**, pp. 277-286, (2004).
18. R. J. S. Brown, Connection between formation factor for electrical-resistivity and fluid-solid coupling factor in Biot equations for acoustic waves in fluid-filled porous media, *Geophysics* **45**, pp. 1269–1275, (1980).
19. COMSOL Multiphysics 3.3a documentation, www.comsol.com.